

Mechanism of Type-II Multiferroicity in Pure and Al-Doped CuFeO_2

Wei qin Zhu,¹ Panshuo Wang,² Haoran Zhu,¹ Haiyan Zhu,¹ Xueyang Li,¹

Jun Zhao,^{1,3} Changsong Xu^{1,3,*} and Hongjun Xiang^{1,†}

¹Key Laboratory of Computational Physical Sciences (Ministry of Education), Institute of Computational Physical Sciences, State Key Laboratory of Surface Physics, and Department of Physics, Fudan University, Shanghai 200433, China

²Key Laboratory of Materials Physics, Ministry of Education, School of Physics, Zhengzhou University, Zhengzhou 450001, China

³Hefei National Laboratory, Hefei 230088, China

 (Received 2 August 2024; revised 23 November 2024; accepted 7 January 2025; published 14 February 2025)

Type-II multiferroicity, where electric polarization is induced by specific spin patterns, is crucial in fundamental physics and advanced spintronics. However, the spin model and magnetoelectric coupling mechanisms in prototypical type-II multiferroic CuFeO_2 and Al-doped CuFeO_2 remain unclear. Here, by considering both spin and alloy degrees of freedom, we develop a magnetic cluster expansion method, which considers all symmetry allowed interactions. Applying such method, we not only obtain realistic spin model that can correctly reproduce observations for both CuFeO_2 and $\text{CuFe}_{1-x}\text{Al}_x\text{O}_2$, but also revisit well-known theories of the original spin-current (SC) model and p - d hybridization model. Specifically, we find that (i) a previously overlooked biquadratic interaction is critical to reproduce the $\uparrow\uparrow\downarrow\downarrow$ ground state and excited states of CuFeO_2 ; (ii) the combination of absent biquadratic interaction and increased magnetic frustration around Al dopants stabilizes the proper screw state; and (iii) it is the generalized spin-current (GSC) model that can correctly characterize the multiferroicity of CuFeO_2 . These findings have broader implications for understanding novel magnetoelectric couplings in, e.g., monolayer multiferroic NiI_2 .

DOI: [10.1103/PhysRevLett.134.066801](https://doi.org/10.1103/PhysRevLett.134.066801)

Type-II multiferroics exhibit electric polarizations induced by spin patterns that break inversion symmetry, leading to strong magnetoelectric coupling and advanced spintronics applications [1–4]. The delafossite compound CuFeO_2 is a prototypical type-II multiferroic, featuring a magnetoelectric mechanism that differs from those with cycloidal magnetism [2,5], making it especially significant for the fundamental physics in the field.

CuFeO_2 crystallizes in the space group $R\bar{3}m$ at room temperature [6,7]. The structure consists of edge-sharing FeO_6 octahedra layers and intervening layers of Cu^+ along the c axis, as shown in Fig. 1(a). The magnetic ions of Fe^{3+} exhibit a d^5 high spin configuration and form a triangular lattice [8–13]. At 11 K, CuFeO_2 undergoes a magnetic transition to the ground state of the collinear four-sublattice (4SL) state, also known as the $\uparrow\uparrow\downarrow\downarrow$ phase [8,14] [see Fig. 1(b)]. A proper screw state emerges when a magnetic field is applied along the out-of-plane direction [7] or when a few percent of Fe ions are substituted with nonmagnetic Al or Ga ions [7,15,16]. This proper screw state propagates along one of the degenerate $\langle 110 \rangle$ axes and induces electric polarization along the parallel direction of propagation [see Fig. 1(c)], resulting in the type-II multiferroic phase.

However, none of the previous models, whether computed from first-principles or fitted from experimental data, have been found to result in the $\uparrow\uparrow\downarrow\downarrow$ phase, let alone the excited states (see details in our results) [17,18]. In the case of $\text{CuFe}_{1-x}\text{Al}_x\text{O}_2$, it is a pity that no model or theory can explain the fact that aluminum substitution down to 2% can lead the system to a helical spin state. Therefore, it is highly desirable to develop new methods and models to correctly describe the magnetism of CuFeO_2 systems, so that their multiferroicity can be accurately understood.

Another issue is that the emergence of polarization in CuFeO_2 is currently not understood. The commonly used theory is the spin-current (SC) model, which links the local electric dipole \mathbf{p} with spins in the form of $\mathbf{p} \propto \mathbf{e}_{ij} \times (\mathbf{S}_i \times \mathbf{S}_j)$, where \mathbf{e}_{ij} is the vector pointing from \mathbf{S}_i to \mathbf{S}_j [19]. This model is successful for the case of TbMnO_3 , where a polarization perpendicular to the propagation direction of the spin cycloid is induced [see Fig. 1(f)]. However, for a proper screw state as in CuFeO_2 , the SC model does not predict a polarization, as \mathbf{e}_{ij} is parallel to $(\mathbf{S}_i \times \mathbf{S}_j)$ [see Fig. 1(g)]. Then, it has been widely believed by many researchers that the spin-dependent hybridization between Fe $3d$ and O $2p$ is responsible for the ferroelectricity [6,20–32]. This p - d hybridization can induce polarization by the charge transfer between metal and ligand with spin-orbit coupling (SOC) effects and a helical spin state [20]. The induced polarization is predicted as

*Contact author: csxu@fudan.edu.cn

†Contact author: hxiang@fudan.edu.cn

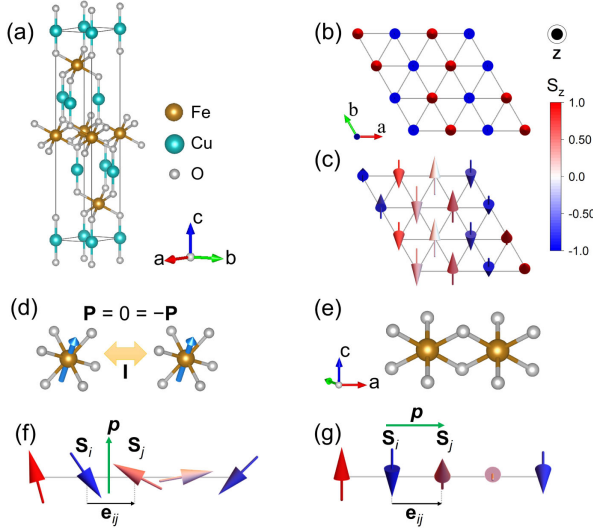


FIG. 1. (a) Crystal structure of CuFeO_2 . (b) Ground state of CuFeO_2 with $\uparrow\uparrow\downarrow\downarrow$ ordering. (c) Ground state of $\text{CuFe}_{1-x}\text{Al}_x\text{O}_2$ showing the helical state, with S_z encoded by color. (d) Spin-order-induced polarization is zero at the spin's spatial inversion center. (e) Nearest neighbor Fe-Fe pair with edge-shared octahedra in CuFeO_2 . (f) Spin cycloid state and electric dipole \mathbf{p} predicted by the SC model. (g) Proper screw state and electric dipole \mathbf{p} predicted by the GSC model.

$\mathbf{p} \propto (\mathbf{e}_{ij} \cdot \mathbf{S}_i)\mathbf{S}_i - (\mathbf{e}_{ij} \cdot \mathbf{S}_j)\mathbf{S}_j$ [20], which lies in the plane spanned by \mathbf{S}_i and \mathbf{S}_j , and is perpendicular to the magnetic propagation vector \mathbf{q} . This contradicts experimental results [7,33] that show $\mathbf{p} \parallel \mathbf{q}$. Thus, p - d hybridization cannot explain the polarization of CuFeO_2 . Therefore, the origin of type-II multiferroicity in CuFeO_2 remains unresolved.

In this Letter, we develop a magnetic cluster expansion method, which is capable of dealing with both spin and alloy (dopant) degrees of freedom and can consider all symmetry-allowed interactions. Applying this method, a realistic model is constructed for $\text{CuFe}_{1-x}\text{Al}_x\text{O}_2$ systems. It is found that, for x choosing its values from zero or finite values, this model not only reproduces the experimental states accurately, but also reveals the critical role of the previously overlooked biquadratic interaction, which arises from metal-ligand-metal superexchange [34,35] (see Sec. XI in Supplemental Material [36]). Additionally, the model shows that Al dopants tilt the delicate balance among different states, resulting in a helical spin state. Furthermore, through symmetry analysis, we find that the multiferroicity of CuFeO_2 can be well explained by a generalized spin-current (GSC) mechanism [37,38].

Magnetic cluster expansion method—To capture the magnetism and multiferroicity in $\text{CuFe}_{1-x}\text{Al}_x\text{O}_2$, we develop an accurate magnetic cluster expansion method. Compared to the spin cluster expansion method [53] and our own symmetry-adapted cluster expansion method [39,54,55], this method explicitly incorporates alloy (dopant) degree of

freedom and its couplings with spin. Notably, symmetry is applied to both spin and alloy degrees of freedom, ensuring all terms in the Hamiltonian are invariants. For $\text{CuFe}_{1-x}\text{Al}_x\text{O}_2$, the effective Hamiltonian can be expressed as

$$\mathcal{H}_{\text{CFAO}} = \mathcal{H}_{\text{CFO}} + \mathcal{H}_{\Delta}, \quad (1)$$

where \mathcal{H}_{CFO} is the spin model of pure CuFeO_2 , while \mathcal{H}_{Δ} denotes the difference arising from Al doping. Typically, one can obtain a realistic model by starting with an initial model with sufficient interactions, where the coefficients can be determined by a machine-learning (ML) method [40] that fits with DFT energies of random spin configurations and random Al doping (see Sec. I in Supplemental Material [36]). The model yields a very small mean average error (MAE) of 0.036 meV/Fe, indicating good accuracy. Note that the Hamiltonian is based on the $R\bar{3}m$ structure, as the monoclinic structural distortion does not impact the main findings (See Sec. VII of Supplemental Material [36]).

Realistic spin model of CuFeO_2 —We first focus on the spin model of pure CuFeO_2 , which is determined as

$$\begin{aligned} \mathcal{H}_{\text{CFO}} = & \sum_{\langle i,j \rangle_n} J_n \mathbf{S}_i \cdot \mathbf{S}_j + \sum_{\langle i,j \rangle_1} B (\mathbf{S}_i \cdot \mathbf{S}_j)^2 \\ & + \sum_{\langle i,j \rangle_1^\perp} J_1^\perp \mathbf{S}_i \cdot \mathbf{S}_j + \sum_i A_{zz} S_i^z S_i^z, \end{aligned} \quad (2)$$

where $\langle i,j \rangle_n$ denotes the n th nearest neighbor (n NN), with $n = 1, 2, 3$, and the superscript \perp represents interlayer interactions. Note that the spin value is set to unity. It is found that the Heisenberg interactions in CuFeO_2 are dominantly antiferromagnetic (AFM), with the strongest coupling being $J_1 = 3.77$ meV, followed by J_3 and J_2 (see Table I). The interlayer coupling $J_1^\perp = 1.04$ meV is also AFM and non-negligible. The relative strengths of these Heisenberg terms are consistent with previous works [17,18]. Moreover, a sizable biquadratic term with $B = -0.92$ meV is predicted for the 1NN, which is absent in previous studies [17,18,31,56,57]. Additionally, the single ion anisotropy (SIA) is found to be of the easy-axis type with $A_{zz} = -0.48$ meV.

To assess the validity of this model, Monte Carlo (MC) simulations and conjugate gradient (CG) optimizations are performed (see Sec. I in Supplemental Material [36]). It turns out that the ground state is indeed the collinear $\uparrow\uparrow\downarrow\downarrow$ state. To elucidate the effects of the biquadratic B term and the $J_1 - J_3$ competition, we construct a phase diagram where J_1, J_2, J_1^\perp , and A_{zz} are kept constant, while J_3 and B are systematically varied. As shown in Fig. 2(a), in the absence of the B term, the system results in a noncollinear state (see Fig. S2 in Supplemental Material [36]), which is in line with the ground states of spin models in previous works [17,18,31,56,57]. On the other hand, increasing J_3

TABLE I. Dominant parameters in $\mathcal{H}_{\text{CFAO}}$, which includes \mathcal{H}_{CFO} and \mathcal{H}_{Δ} . $|\mathbf{S}| = 1$ is adopted for better parameter comparison. Energy unit is in meV.

\mathcal{H}_{CFO}				\mathcal{H}_{Δ}			
J_1	3.77	J_2	1.13	J_3	1.81	$\Delta J_{3,6}$	1.20
J_1^\perp	1.04	B	-0.92	A_{zz}	-0.48	$\Delta J_{3,7}$	0.37

(resulting in a stronger J_3/J_1) leads to the stabilization of an incommensurate helical state propagating along the $\langle 110 \rangle$ directions, denoted as IC⁽¹¹⁰⁾.

Furthermore, the model \mathcal{H}_{CFO} accurately describes the excited states, which are investigated by applying a magnetic field along the c axis. As shown in Fig. 2(b), for a field stronger than 24 T, a proper screw state emerges. This state propagates along equivalent $\langle 110 \rangle$ directions and possesses a similar energy (only 0.06 meV/Fe higher) than the $\uparrow\uparrow\downarrow$ state, consistent with experimental results. It is found that slightly weakening the value of B makes the proper screw state more energetically favorable, confirming the critical role of the biquadratic term in stabilizing the $\uparrow\uparrow\downarrow$ state. Further increasing the field beyond 26 T, the proper screw state transforms into the so-called five-sublattice $\uparrow\uparrow\uparrow\downarrow$ state. Note that the $\langle 110 \rangle$ helical state breaks inversion symmetry and induces electric polarization. In addition to the field effects, the transition from ordered magnetism to paramagnetism at finite temperatures is also well reproduced by our effective model, as shown in Fig. 2(b). The good agreement between our simulations and experimental measurements [7,58,59] confirms the high accuracy of our model and emphasizes the significance of the biquadratic B term.

Effective model of CuFe_{1-x}Al_xO₂—We now turn to examine the effects of Al dopants, i.e., CuFe_{1-x}Al_xO₂ with x being finite. In the present case, we consider the changes in spin interactions, with at least one Fe being the first nearest neighbor to Al dopant. Then, the model of $\mathcal{H}_{\text{CFAO}}$ is obtained from fitting, and the part resulted from Al doping reads

$$\mathcal{H}_{\Delta} = \sum_{\langle i,j \rangle_{n,k}} \Delta J_{n,k} \mathbf{S}_i \cdot \mathbf{S}_j, \quad (3)$$

where ΔJ represents changes in the Heisenberg interactions in the proximity of Al dopants. The neighboring index n ranges from 1 to 3, and index k denotes the geometry between the Fe-Fe pair and the Al dopant [see examples in Fig. 3(c) and details in Table S3 [36]]. Among the various doping-induced modifications to the Heisenberg interactions, $\Delta J_{3,6} = 1.20$ and $\Delta J_{3,7} = 0.37$ meV are the dominant ones, both enhancing the original J_3 . Other parameters are found to contribute much less to the formation of proper screw [60]. Note that the enhancement of J_3 roots in the increased of e_g - e_g hopping near the Al

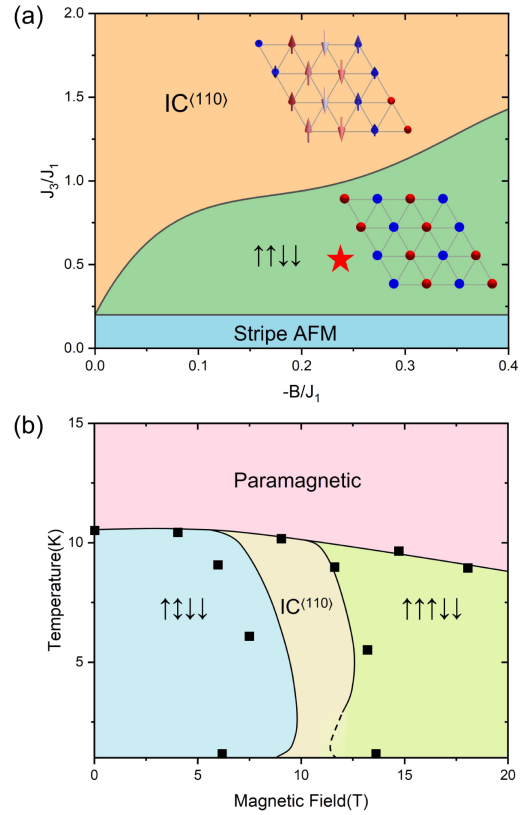


FIG. 2. (a) Phase diagram for a triangular lattice system with varied J_3 and B , using fixed parameters: $J_1 = 1$ meV (AFM), $J_2 = 0.30$ meV, $J_1^\perp = 0.27$ meV, $A_{zz} = -0.13$ meV, $J_3 > 0$, and $B < 0$. The red star indicates pure CuFeO₂. The S_z component is shown by a color gradient on the vectors [see Fig. 1(b) for the color bar]. (b) Field-temperature phase diagram of the model \mathcal{H}_{CFO} , with black squares representing measured data [9]. The dashed line indicates the coexistence of IC⁽¹¹⁰⁾ and $\uparrow\uparrow\uparrow\downarrow$ states. Horizontal and vertical axes are rescaled by factors of 0.4 and 0.5, respectively, for better comparison with experimental data (see Sec. IX in Supplemental Material [36]).

dopant (see Sec. VI in Supplemental Material [36]). Notably, we find that the influence of Al on SIA, J_1^\perp , B and Dzyaloshinskii-Moriya interaction is sufficiently weak and can thus be neglected (see Sec. III in Supplemental Material [36]).

To verify the accuracy of our model, we perform MC and CG simulations on supercells with and without Al dopants using the Hamiltonian of $\mathcal{H}_{\text{CFAO}}$, as in Eq. (1). When doping concentration is zero, the model reduce to \mathcal{H}_{CFO} . When doping Al around the density of $x = 0.02$, the system enters a mixed state combining $\uparrow\uparrow\downarrow$ phase and a helical phase, as shown in Fig. 3(a). This mixed state aligns well with experimental observations. The pure helical state gradually lowers its energy with respect to the $\uparrow\uparrow\downarrow$ state and becomes ground state for $x > 0.07$ (see Fig. S10 of Supplemental Material [36]). The helical phase propagates along lattice vector \mathbf{a} direction (x direction in Fig. 3), which

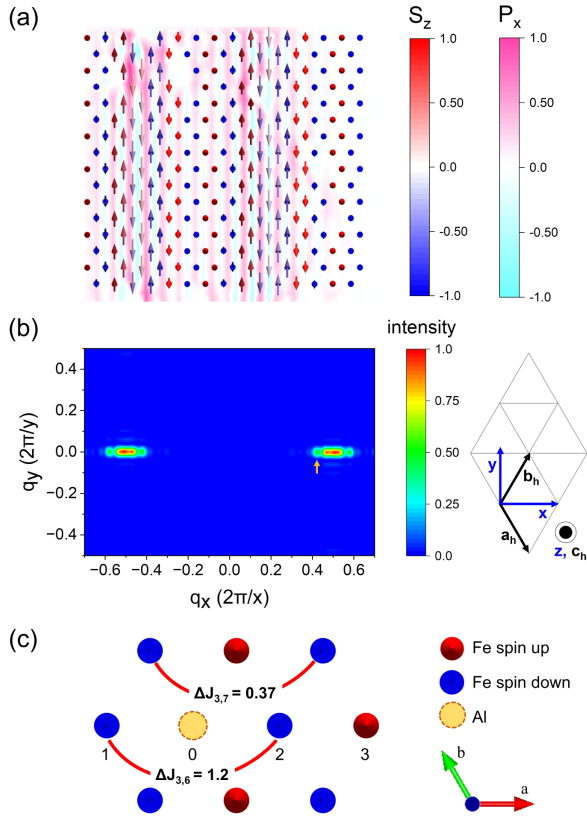


FIG. 3. (a) Spin configurations for $\text{CuFe}_{1-x}\text{Al}_x\text{O}_2$ with $x = 0.02$. The x component of induced electric polarization is shown in magenta-cyan. (b) Spin structure factor $S(q)$ for the spin pattern in (a), with the peak at $q_x = 0.42$ marked by a yellow arrow, corresponding to the proper screw in (a). (c) Mechanism for the emergence of the helical state in $\text{CuFe}_{1-x}\text{Al}_x\text{O}_2$. Two dominant ΔJ (see Table I) are marked by solid lines. Note that the red line shows a 1.2 and 0.37 meV increase in J_3 due to Al doping.

is equivalent to $\langle 110 \rangle$ directions, i.e. the $\text{IC}^{(110)}$ state. To determine the period of the helical state, we calculate the spin structure factor, which is defined as $S_q = (1/N) \sum_{\alpha=x,y,z} \langle |\sum_{i,\alpha} S_{i,\alpha} e^{-i\mathbf{q}\cdot\mathbf{r}_i}|^2 \rangle$ [61]. The $\uparrow\uparrow\downarrow\downarrow$ phase corresponds to a pair of bright spots at $\mathbf{q} = (\pm 0.5, 0, 0)$ (see Fig. S3 in Supplemental Material [36]); While the mixed state not only shows two major spots near zone boundary ($q_x = \pm 0.5$), but also exhibits two more spots at $\mathbf{q} = (\pm 0.42, 0, 0)$, as shown in Fig. 3(b). Such latter spots corresponds to the helical state and indicate an averaged period of $2.38a$. The propagation direction and period of the helical state are both consistent with measurements (2.41a) [16,58,59], indicating a good accuracy of our model. Moreover, the present method allows for varying the concentration x and demonstrates a larger proportion of the helical state with an increase in x (see Fig. S5 in Supplemental Material [36]).

We now turn to unravel the mechanisms that induce the emergence of the $\text{IC}^{(110)}$ helical spin state. Starting with

\mathcal{H}_{CFO} , we introduce Al dopants and gradually incorporate different $\Delta J_{n,k}$ terms and exam the resulted phases. Results from these tests indicate that (i) the $\text{IC}^{(110)}$ state does not emerge solely with the presence of Al dopants but without changing any parameters; while (ii) if $\Delta J_{3,6}$ ($\Delta J_{3,7}$, respectively) is considered, the $\text{IC}^{(110)}$ state begins to emerge for $x \geq 0.05$ ($x \geq 0.04$, respectively). If incorporating all non-negligible $\Delta J_{n,k}$ terms, the critical concentration decreases to $x \approx 0.02$ (see Fig. S6 in Supplemental Material [36]). We then choose two states: a $\uparrow\uparrow\downarrow\downarrow$ state and a mixed state with both $\uparrow\uparrow\downarrow\downarrow$ and $\text{IC}^{(110)}$ patterns, and decompose their energy into contributions from each considered term. It is found that, compared to the $\uparrow\uparrow\downarrow\downarrow$ state, the $\Delta J_{3,6}$ and $\Delta J_{3,7}$ terms favor the $\text{IC}^{(110)}$ state and primarily contribute to energy gains of -0.017 and -0.024 meV/Fe, respectively. Notably, although the value of $\Delta J_{3,7}$ is smaller than $\Delta J_{3,6}$, it has higher pair multiplicity [refer to Fig. 3(c)] and thus contributes the most energy gain. In contrast, other $\Delta J_{n,k}$ terms with modest values contribute negligible energy gain or cost. On another aspect, the presence of Al eliminates biquadratic interactions (which favor collinear alignments) in the nearby area, thereby promoting noncollinear states. It is thus demonstrated that the emergence of $\text{IC}^{(110)}$ state is due to the enhancement in J_3 (stronger $J_1 - J_3$ competition) and absence of biquadratic interactions induced by Al doping.

Origin of multiferroicity in CuFeO_2 —We now investigate the origin of the ferroelectricity in CuFeO_2 induced by spin order. According to the discussion in the introduction, the original SC model and the p - d hybridization theorem does not work for CuFeO_2 . For the invalidity of the p - d hybridization theorem, it is easy to understand that the spins on Fe ions are actually located at inversion centers, which do not generate any polar quantities [see Fig. 1(d) and Sec. V in Supplemental Material [36]]. We thus turn to the GSC model [37,38], according to which the local polarization induced by spins \mathbf{S}_i and \mathbf{S}_j can be expressed as $\mathbf{P}_{ij} = \mathcal{M}(\mathbf{S}_i \times \mathbf{S}_j)$, where matrix \mathcal{M} can be extracted from DFT calculations using the four-state method [37]. For the nearest neighbor Fe-Fe pair along the direction of lattice vector \mathbf{a} , it yields

$$\mathcal{M} = \begin{bmatrix} M_{11} & 0 & 0 \\ 0 & M_{22} & M_{23} \\ 0 & M_{32} & M_{33} \end{bmatrix}, \quad (4)$$

where $M_{11} = 16.75$, $M_{22} = -99.5$, $M_{23} = -49.5$, $M_{32} = 79.5$, $M_{33} = 47.5$ in unit of $10^{-5} e \cdot \text{\AA}$. This form of \mathcal{M} is consistent with the local C_{2h} symmetry of the adopted Fe-Fe pair [see Fig. 1(e)]. Applying GSC model with \mathcal{M} in Eq. (4), the spin induced electric polarization is calculated for CuFeO_2 . As shown in Fig. 3(a) (see also Fig. S3 in Supplemental Material [36]), there is no

polarization near the collinear $\uparrow\uparrow\downarrow\downarrow$ state, while a net $P_x > 0$ is observed in the proper screw area, which is consistent with measurements that \mathbf{P} is parallel to spin propagation direction [7]. The simulated value yields $177 \mu\text{C}/\text{m}^2$ for $x = 0.02$ doping, which agrees well with measured $140 \mu\text{C}/\text{m}^2$ [62], indicating the validity of GSC model. Moreover, we find that the failure of usual SC model for CuFeO_2 is actually due to that its form of $\mathbf{p} \propto \mathbf{e}_{ij} \times (\mathbf{S}_i \times \mathbf{S}_j)$ actually neglects diagonal elements of \mathcal{M} matrix, especially M_{11} for CuFeO_2 (see Sec. V in Supplemental Material [36]).

In summary, we newly develop a first-principles-based symmetry-adapted magnetic cluster expansion method, which can consider both spin and alloy (dopant) degrees of freedom. For pure CuFeO_2 , our model indicates that the overlooked biquadratic interaction is necessary to reproduce the $\uparrow\uparrow\downarrow\downarrow$ ground state. For $\text{CuFe}_{1-x}\text{Al}_x\text{O}_2$, it correctly predicts the helical ground state and its magnetic propagation vector, primarily due to Al-induced absence of biquadratic interaction and enhancements in the third nearest neighbor antiferromagnetic coupling. Furthermore, we show that the multiferroicity in CuFeO_2 can be well described by the generalized spin-current mechanism, instead of commonly believed p - d hybridization. Notably, the spin structure of CuFeO_2 is similar to that of the 2D type-II multiferroics NiI_2 [41,42,63] and MnI_2 [64], suggesting a comparable magnetoelectric mechanism in these layered systems. Our Letter clarifies the mechanisms of magnetism and ferroelectricity in CuFeO_2 systems, and has significant implications for the highly regarded field of two-dimensional multiferroics.

Acknowledgments—We acknowledge financial support from NSFC (Grants No. 12188101, No. 12174060, and No. 12274082, the National Key R&D Program of China (No. 2022YFA1402901), the Guangdong Major Project of the Basic and Applied basic Research (Future functional materials under extreme conditions—C2021B0301030005), Shanghai Pilot Program for Basic Research—FuDan University 21TQ1400100 (23TQ017), and Shanghai Science and Technology Program (23JC1400900). C. X. also acknowledges support from the Shanghai Science and Technology Committee (Grant No. 23ZR1406600), Innovation Program for Quantum Science and Technology (2024ZD0300102) and the Xiaomi Young Talents Program. J. Z. was supported by the Key Program of the National Natural Science Foundation of China (Grant No. 12234006).

-
- [1] S. Dong, H. Xiang, and E. Dagotto, Magnetoelectricity in multiferroics: A theoretical perspective, *Natl. Sci. Rev.* **6**, 629 (2019).
 [2] T. Kimura, T. Goto, H. Shintani, K. Ishizaka, T. Arima, and Y. Tokura, Magnetic control of ferroelectric polarization, *Nature (London)* **426**, 55 (2003).

- [3] S. Emori, U. Bauer, S.-M. Ahn, E. Martinez, and G. S. D. Beach, Current-driven dynamics of chiral ferromagnetic domain walls, *Nat. Mater.* **12**, 611 (2013).
 [4] D.-L. Bao, A. O'Hara, S. Du, and S. T. Pantelides, Tunable, ferroelectricity-inducing, spin-spiral magnetic ordering in monolayer FeOCl , *Nano Lett.* **22**, 3598 (2022).
 [5] Y. J. Choi, H. T. Yi, S. Lee, Q. Huang, V. Kiryukhin, and S.-W. Cheong, Ferroelectricity in an Ising chain magnet, *Phys. Rev. Lett.* **100**, 047601 (2008).
 [6] Y. Tanaka, N. Terada, T. Nakajima, M. Taguchi, T. Kojima, Y. Takata, S. Mitsuda, M. Oura, Y. Senba, H. Ohashi, and S. Shin, Incommensurate orbital modulation behind ferroelectricity in CuFeO_2 , *Phys. Rev. Lett.* **109**, 127205 (2012).
 [7] S. Seki, Y. Yamasaki, Y. Shiomi, S. Iguchi, Y. Onose, and Y. Tokura, Impurity-doping-induced ferroelectricity in the frustrated antiferromagnet CuFeO_2 , *Phys. Rev. B* **75**, 100403(R) (2007).
 [8] F. Ye, Y. Ren, Q. Huang, J. A. Fernandez-Baca, P. Dai, J. W. Lynn, and T. Kimura, Spontaneous spin-lattice coupling in the geometrically frustrated triangular lattice antiferromagnet CuFeO_2 , *Phys. Rev. B* **73**, 220404(R) (2006).
 [9] T. Kimura, J. C. Lashley, and A. P. Ramirez, Inversion-symmetry breaking in the noncollinear magnetic phase of the triangular-lattice antiferromagnet CuFeO_2 , *Phys. Rev. B* **73**, 220401(R) (2006).
 [10] H.-W. Chen, C.-Y. Huang, G.-J. Shu, and H.-L. Liu, Temperature-dependent optical properties of CuFeO_2 through the structural phase transition, *RSC Adv.* **11**, 40173 (2021).
 [11] Q. Song *et al.*, Growth of PdCoO_2 films with controlled termination by molecular-beam epitaxy and determination of their electronic structure by angle-resolved photoemission spectroscopy, *APL Mater.* **10**, 091113 (2022).
 [12] D. Dong, K. Xiao-Yu, G. Jian-Jun, W. Hui, and Z. Kang-Wei, Optical absorption and epr study of the octahedral Fe^{3+} center in yttrium aluminum garnet, *Phys. Rev. B* **72**, 073101 (2005).
 [13] D. M. Pajerowski, Mixing A-type and G-type B-site antiferromagnetism in $\text{AMn}_{1-x}\text{Fe}_x\text{O}_3$ ($A = \text{La, Nd}$), *Phys. Rev. B* **98**, 134431 (2018).
 [14] S. Mitsuda, Y. Matsumoto, T. Wada, K. Kurihara, Y. Urata, H. Yoshizawa, and M. Mekata, Magnetic ordering of $\text{CuFe}_{1-x}\text{Al}_x\text{O}_2$, *Physica (Amsterdam)* **213–214B**, 194 (1995).
 [15] N. Terada, S. Mitsuda, K. Prokes, O. Suzuki, H. Kitazawa, and H. A. Katori, Impact of a small number of nonmagnetic impurities on H-T magnetic phase diagram of CuFeO_2 , *Phys. Rev. B* **70**, 174412 (2004).
 [16] N. Terada, S. Mitsuda, T. Fujii, K.-i. Soejima, I. Doi, H. Aruga Katori, and Y. Noda, Magnetic phase diagram of the triangular lattice antiferromagnet $\text{CuFe}_{1-x}\text{Al}_x\text{O}_2$, *J. Phys. Soc. Jpn.* **74**, 2604 (2005).
 [17] F. Ye, J. A. Fernandez-Baca, R. S. Fishman, Y. Ren, H. J. Kang, Y. Qiu, and T. Kimura, Magnetic interactions in the geometrically frustrated triangular lattice antiferromagnet CuFeO_2 , *Phys. Rev. Lett.* **99**, 157201 (2007).
 [18] Y. Zhang, E. Kan, and M.-H. Whangbo, Density functional investigation of the difference in the magnetic structures of the layered triangular antiferromagnets CuFeO_2 and AgCrO_2 , *Chem. Mater.* **23**, 4181 (2011).

- [19] H. Katsura, N. Nagaosa, and A. V. Balatsky, Spin current and magnetoelectric effect in noncollinear magnets, *Phys. Rev. Lett.* **95**, 057205 (2005).
- [20] T.-h. Arima, Ferroelectricity induced by proper-screw type magnetic order, *J. Phys. Soc. Jpn.* **76**, 073702 (2007).
- [21] J.-M. L. K. F. Wang and Z. Ren, Multiferroicity: The coupling between magnetic and polarization orders, *Adv. Phys.* **58**, 321 (2009).
- [22] R. S. Fishman, Phase diagram of a geometrically frustrated triangular-lattice antiferromagnet in a magnetic field, *Phys. Rev. Lett.* **106**, 037206 (2011).
- [23] K. Singh, A. Maignan, C. Martin, and C. Simon, AgCrS₂: A spin driven ferroelectric, *Chem. Mater.* **21**, 5007 (2009).
- [24] Y. Tokura and N. Nagaosa, Nonreciprocal responses from non-centrosymmetric quantum materials, *Nat. Commun.* **9**, 3740 (2018).
- [25] M. Mostovoy, Multiferroics: Different routes to magnetoelectric coupling, *npj Spintron.* **2**, 18 (2024).
- [26] Y. Narumi, T. Nakamura, H. Ikeno, N. Terada, T. Morioka, K. Saito, H. Kitazawa, K. Kindo, and H. Nojiri, Evidence of charge transfer and orbital magnetic moment in multiferroic CuFeO₂, *J. Phys. Soc. Jpn.* **85**, 114705 (2016).
- [27] C. Jia, S. Onoda, N. Nagaosa, and J. H. Han, Bond electronic polarization induced by spin, *Phys. Rev. B* **74**, 224444 (2006).
- [28] S. Seki, N. Kida, S. Kumakura, R. Shimano, and Y. Tokura, Electromagnons in the spin collinear state of a triangular lattice antiferromagnet, *Phys. Rev. Lett.* **105**, 097207 (2010).
- [29] S. Luo, K. F. Wang, S. Z. Li, X. W. Dong, Z. B. Yan, H. L. Cai, and J.-M. Liu, Enhanced ferromagnetism and ferroelectricity in multiferroic CuCr_{1-x}Ni_xO₂, *Appl. Phys. Lett.* **94**, 172504 (2009).
- [30] T. Nakajima *et al.*, Comprehensive study on ferroelectricity induced by a proper-screw-type magnetic ordering in multiferroic CuFeO₂: Nonmagnetic impurity effect on magnetic and ferroelectric order, *Phys. Rev. B* **79**, 214423 (2009).
- [31] J. T. Haraldsen, F. Ye, R. S. Fishman, J. A. Fernandez-Baca, Y. Yamaguchi, K. Kimura, and T. Kimura, Multiferroic phase of doped delafossite CuFeO₂ identified using inelastic neutron scattering, *Phys. Rev. B* **82**, 020404(R) (2010).
- [32] N. Terada, Spin and orbital orderings behind multiferroicity in delafossite and related compounds, *J. Phys. Condens. Matter* **26**, 453202 (2014).
- [33] T. Nakajima, S. Mitsuda, S. Kanetsuki, K. Tanaka, K. Fujii, N. Terada, M. Soda, M. Matsuura, and K. Hirota, Electric polarization induced by a proper helical magnetic ordering in a delafossite multiferroic CuFe_{1-x}Al_xO₂, *Phys. Rev. B* **77**, 052401 (2008).
- [34] A. Kartsev, M. Augustin, R. F. L. Evans, K. S. Novoselov, and E. J. G. Santos, Biquadratic exchange interactions in two-dimensional magnets, *npj Comput. Mater.* **6**, 150 (2020).
- [35] J. Y. Ni, X. Y. Li, D. Amoroso, X. He, J. S. Feng, E. J. Kan, S. Picozzi, and H. J. Xiang, Giant biquadratic exchange in 2d magnets and its role in stabilizing ferromagnetism of NiCl₂ monolayers, *Phys. Rev. Lett.* **127**, 247204 (2021).
- [36] See Supplemental Material at <http://link.aps.org/supplemental/10.1103/PhysRevLett.134.066801> which includes Refs. [8,17,18,34,35,37–52] for detailed methods and further discussions.
- [37] H. J. Xiang, E. J. Kan, Y. Zhang, M.-H. Whangbo, and X. G. Gong, General theory for the ferroelectric polarization induced by spin-spiral order, *Phys. Rev. Lett.* **107**, 157202 (2011).
- [38] P. Wang, X. Lu, X. Gong, and H. Xiang, Microscopic mechanism of spin-order induced improper ferroelectric polarization, *Comput. Mater. Sci.* **112**, 448 (2016).
- [39] F. Lou, X. Y. Li, J. Y. Ji, H. Y. Yu, J. S. Feng, X. G. Gong, and H. J. Xiang, PASP: Property analysis and simulation package for materials, *J. Chem. Phys.* **154**, 114103 (2021).
- [40] X.-Y. Li, F. Lou, X.-G. Gong, and H. Xiang, Constructing realistic effective spin Hamiltonians with machine learning approaches, *New J. Phys.* **22**, 053036 (2020).
- [41] Q. Song *et al.*, Evidence for a single-layer van der Waals multiferroic, *Nature (London)* **602**, 601 (2022).
- [42] X. Li, C. Xu, B. Liu, X. Li, L. Bellaïche, and H. Xiang, Realistic spin model for multiferroic NiI₂, *Phys. Rev. Lett.* **131**, 036701 (2023).
- [43] G. Kresse and J. Furthmüller, Efficient iterative schemes for *ab initio* total-energy calculations using a plane-wave basis set, *Phys. Rev. B* **54**, 11169 (1996).
- [44] P. E. Blöchl, Projector augmented-wave method, *Phys. Rev. B* **50**, 17953 (1994).
- [45] J. P. Perdew, K. Burke, and M. Ernzerhof, Generalized gradient approximation made simple, *Phys. Rev. Lett.* **77**, 3865 (1996).
- [46] A. I. Liechtenstein, V. I. Anisimov, and J. Zaanen, Density-functional theory and strong interactions: Orbital ordering in Mott-Hubbard insulators, *Phys. Rev. B* **52**, R5467 (1995).
- [47] M. R. Hestenes, E. Stiefel *et al.*, Methods of conjugate gradients for solving linear systems, *J. Res. Natl. Bur. Stand.* **49**, 409.
- [48] C. Xu, J. Feng, S. Prokhorenko, Y. Nahas, H. Xiang, and L. Bellaïche, Topological spin texture in Janus monolayers of the chromium trihalides Cr(I,X)₃, *Phys. Rev. B* **101**, 060404(R) (2020).
- [49] X. He, N. Helbig, M. J. Verstraete, and E. Bousquet, TB2J: A python package for computing magnetic interaction parameters, *Comput. Phys. Commun.* **264**, 107938 (2021).
- [50] T. Zakrzewski and P. Boguslawski, Electronic structure of transition metal ions in GaN and AlN: Comparing GGA + U with experiment, *J. Alloys Compd.* **664**, 565 (2016).
- [51] A. Kartsev, O. D. Feyta, N. Bondarenko, and A. G. Kvashnin, Stability and magnetism of FeN high-pressure phases, *Phys. Chem. Chem. Phys.* **21**, 5262 (2019).
- [52] B. Mnisi, E. Benecha, and M. Tibane, Density functional theory studies of structural, electronic and optical properties of cubic 3d-transition metal nitrides, *Intermetallics* **137**, 107272 (2021).
- [53] R. Drautz and M. Fähnle, Spin-cluster expansion: Parametrization of the general adiabatic magnetic energy surface with *ab initio* accuracy, *Phys. Rev. B* **69**, 104404 (2004).
- [54] C. Xu, X. Li, P. Chen, Y. Zhang, H. Xiang, and L. Bellaïche, Assembling diverse skyrmionic phases in Fe₃GeTe₂ monolayers, *Adv. Mater.* **34**, 2107779 (2022).
- [55] C. Xu, H. Yu, J. Wang, and H. Xiang, First-principles approaches to magnetoelectric multiferroics, *Annu. Rev. Condens. Matter Phys.* **15**, 85 (2024).
- [56] O. Petrenko, M. Lees, G. Balakrishnan, S. De Brion, and G. Chouteau, Revised magnetic properties of CuFeO₂ a case of

- mistaken identity, *J. Phys. Condens. Matter* **17**, 2741 (2005).
- [57] A. Apostolov, I. Apostolova, and J. Wesselinowa, Ferroelectricity in the multiferroic delafossite CuFeO_2 induced by ion doping or magnetic field, *Solid State Commun.* **292**, 11 (2019).
- [58] S. Kanetsuki, S. Mitsuda, T. Nakajima, D. Anazawa, H. A. Katori, and K. Prokes, Field-induced ferroelectric state in frustrated magnet $\text{CuFe}_{1-x}\text{Al}_x\text{O}_2$, *J. Phys. Condens. Matter* **19**, 145244 (2007).
- [59] T. Nakajima, S. Mitsuda, T. Inami, N. Terada, H. Ohsumi, K. Prokes, and A. Podlesnyak, Identification of microscopic spin-polarization coupling in the ferroelectric phase of magnetoelectric multiferroic $\text{CuFe}_{1-x}\text{Al}_x\text{O}_2$, *Phys. Rev. B* **78**, 024106 (2008).
- [60] Other non-negligible parameters include $\Delta J_{1,1} = -0.24$, $\Delta J_{1,2} = 0.33$, $\Delta J_{1,3} = 0.94$ and $\Delta J_{2,4} = 0.59$ meV, but they contribute much less to the formation of proper screw due to geometric configurations and smaller pair multiplicity.
- [61] D. Amoroso, P. Barone, and S. Picozzi, Spontaneous skyrmionic lattice from anisotropic symmetric exchange in a Ni-halide monolayer, *Nat. Commun.* **11**, 5784 (2020).
- [62] T. Nakajima *et al.*, Anisotropic magnetic field responses of ferroelectric polarization in the trigonal multiferroic $\text{CuFe}_{1-x}\text{Al}_x\text{O}_2$ ($x = 0.015$), *Phys. Rev. B* **81**, 014422 (2010).
- [63] T. Kurumaji, S. Seki, S. Ishiwata, H. Murakawa, Y. Kaneko, and Y. Tokura, Magnetoelectric responses induced by domain rearrangement and spin structural change in triangular-lattice helimagnets NiI_2 and CoI_2 , *Phys. Rev. B* **87**, 014429 (2013).
- [64] T. Kurumaji, S. Seki, S. Ishiwata, H. Murakawa, Y. Tokunaga, Y. Kaneko, and Y. Tokura, Magnetic-field induced competition of two multiferroic orders in a triangular-lattice helimagnet MnI_2 , *Phys. Rev. Lett.* **106**, 167206 (2011).